Polymer Chemistry

ROYAL SOCIETY OF CHEMISTRY

PAPER

Check for updates

Amphiphilic poly(esteracetal)s as dual pH- and enzyme-responsive micellar immunodrug delivery systems†

Leon Bixenmann, Judith Stickdorn and Lutz Nuhn ●ID *

Poly(esteracetal)s are equipped with both acid-labile acetal and base-labile ester functionalities in their backbone, thus, providing dual pH-responsive degradation profiles. In this study, the cyclic esteracetal monomer 2-methyl-1,3-dioxan-4-one (MDO) was polymerised *via* a cationic ring-opening mechanism onto methoxy poly(ethylene glycol) (mPEG) affording amphiphilic mPEG-*b*-P(MDO) poly(esteracetal) block copolymers that self-assemble into well-defined monomodal micelles by direct hydration with aqueous buffers. Their pH-responsive behaviour towards rapid particle degradation was confirmed by DLS and ^{1}H-NMR. Upon acidification or basification and lipase-mediated enzymatic hydrolysis, immediate polymer degradation and cargo release could be observed. As an example for further suitable applications, an amphiphilic immune stimulatory TLR-7 agonist (Adifectin) was co-formulated into mPEG-*b*-P(MDO) block copolymer micelles and its activity was investigated by TLR stimulation of RAW Blue macrophages. The degradable amphiphilic block copolymer was able to solubilize the drug more efficiently and retained its receptor activity. Consequently, mPEG-*b*-P(MDO) based amphiphilic poly(esteracetal)s can be considered as promising delivery systems for further immunodrugs and, thus, may contribute towards improving their translatability.

1. Introduction

Delivering pharmaceutically active molecules to their specific therapeutic target by using nanosized carrier systems has attracted major interest to overcome current limitations of drug therapies.[1,2] Many hydrophobic drugs suffer from low solubility and unspecific binding which cause non-controllable toxicities.[3,4] This includes novel promising anticancer or immune therapeutics which accumulate insufficiently at their target sites. As a result, their related off-target effects limit any clinical translatability. In that context, amphiphilic block copolymers may support the drugs when formulated into nanometre-sized micellar delivery systems. They are structurally composed of a hydrophilic corona and a hydrophobic core where the therapeutic compounds can be entrapped physically.[2,5–7] The size, surface properties and responsive behaviour of the micelles can determine the accessibility and tissue accumulation of drugs.[8] Many attempts have been made to translate this general principle into clinical practice including paclitaxel formulations such as Genexol-PM, which was approved in 2007 in South Korea for breast cancer.[4,7,9]

In parallel, novel therapeutic antitumour concepts have evolved over the last decade, especially with respect to the role of the immune system in cancer progression. Scientists envision reinforcing immune reactions against cancer cells by delivering immune-stimulating therapeutics to the tumour microenvironment and its draining lymph nodes.[6,10] Immunostimulants such as the Toll-like receptor (TLR) 7 agonist imiquimod are highly potent in inducing innate immune responses and result in an activation of a broad spectrum of antigen-presenting cells and sufficient activation of cytotoxic T-cells. Unfortunately, if administered systemically, uncontrolled inflammations are elicited also in healthy tissues leading to severe side effects.[11] To overcome these dose-limiting toxicities, nanocarriers are considered as ideal delivery vehicles especially for such small molecular immunotherapeutics, *e.g.* to enhance their transport, release and activity in the lymph nodes.[12–14] Consequently, a fundamental challenge is to design carriers with sufficient tissue mobility to lymph nodes that show at the same time appropriate uptake by relevant immune cells.

Recently reported findings imply that lymph nodes can exhibit acidic compartments that inhibit T-cell effector functions.[15] Therefore, an acid triggered cleavage of the shielding

Max Planck Institute for Polymer Research, Ackermannweg 10, 55128 Mainz, Germany. E-mail: lutz.nuhn@mpip-mainz.mpg.de; Tel: +49 (0) 6131-379-311
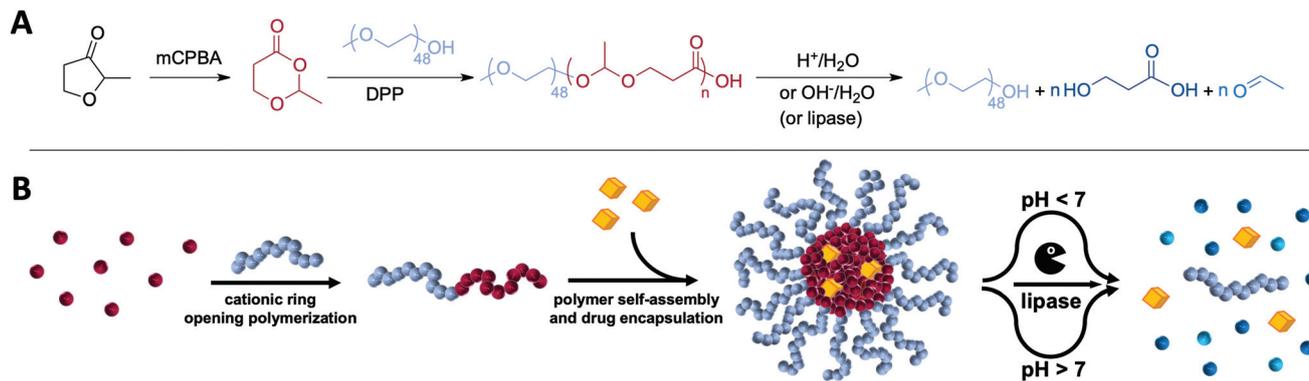†Electronic supplementary information (ESI) available. See DOI: 10.1039/c9py01716j

Fig. 1 (A) Synthesis and dual pH-responsive (or enzymatic) degradation of amphiphilic poly(esteracetal) block copolymers. (B) Schematic illustration of the concept using amphiphilic poly(esteracetal) block copolymers and their derived micelles for pH- and lipase-responsive delivery of immunodrugs.

corona followed by the release of immunotherapeutics might be a beneficial strategy towards lymph node targeted delivery of immune stimulatory drugs. As advanced multi-responsive class of materials, poly(esteracetal)s can provide such acid-cleavable features beyond classical ester hydrolysis (the latter commonly guarantees avoiding long-term particle accumulation by *e.g.* enzyme-mediated ester cleavage).

Poly(esteracetal)s are accessible by ring-opening polymerisation and are gaining growing interest especially towards the development of degradable polymers for sustainable plastics.[16–18] In this respect, Hillmyer and coworkers have recently provided major contributions to a mechanistic understanding of their fabrication.[17,18] In one of their seminal works, Hillmyer *et al.* applied cationic ring-opening polymerisation conditions to cyclic ester acetal monomers which prevented the expulsion of acetaldehyde.[18] Using the acidic organocatalyst diphenyl phosphoric acid (DPP), they showed successful poly(esteracetal) formation with different end groups based on the applied alcohol initiator. However, to the best of our knowledge, a block copolymerisation with macro-initiators towards amphiphilic diblock copolymers has so far not been reported.

With the expansion of classical micellar drug carrier systems, we believe that micelles derived from poly(esteracetal) diblock copolymers are a promising platform for lymph node-responsive delivery of immunotherapeutics. The acid-degradable acetal group ensures rapid carrier degradation and cargo release in acidic environments such as in immunosuppressive cancers and their draining lymph nodes, while the ester functionalities further enable long-term enzymatic carrier clearance from the body. In this context, our work aims at providing first proof-of-concept studies on applying amphiphilic poly(esteracetal)s in immunodrug delivery. In this respect, the reported synthesis of poly(esteracetal) homopolymers initiated by small molecular alcohols was adopted and successfully modified towards amphiphilic block copolymerisation by using mPEG as a macroinitiator. The self-assembly behaviour of the resulting block copolymers was carefully investigated in

aqueous media. Thereby, the dual pH-responsive and enzymatic degradation profiles of the polymers and their derived micelles could be confirmed by NMR spectroscopy, size exclusion chromatography and dynamic light scattering. To demonstrate the ability of solubilizing hydrophobic drug compounds, poly(esteracetal) micelles were loaded with a hydrophobic dye and an amphiphilic immune stimulatory TLR7 agonist. Primary *in vitro* cell studies revealed low carrier toxicities and successful TLR7 stimulation for the drug-loaded micelles (Fig. 1). Altogether, our findings confirm the high potential of amphiphilic poly(esteracetal)s in immunodrug delivery and may contribute towards improving the translatability of further promising immunodrugs.

2. Experimental section

2.1 Materials

Unless otherwise stated, all reagents were purchased from Sigma-Aldrich or Fisher Scientific. 1,2-Dichloroethane (DCE) and dichloromethane (DCM) as solvents were dried by heating under reflux over calcium hydride for 3 h, and then stirred overnight at room temperature and distilled prior to use. The cyclic esteracetal monomer 2-methyl-1,3-dioxan-4-one (MDO) was synthesized from commercial 2-methyltetrahydrofuran-3-one, as has recently been reported.[17] Prior to use, MDO was dried over calcium hydride overnight at room temperature (rt) and freshly distilled. Magnesium sulphate was obtained from Acros Organics and diphenylphosphoric acid (DPP) was purchased from Alfa Aesar. DPP was dried under high vacuum (0.05 mbar) overnight. DPP-catalyst stock solutions were prepared from dried DPP in either anhydrous 1,2-dichloroethane or dichloromethane. Polyethylene glycol was purchased from Fluka® Analytical. Prior to use, it was also dried by azeotropic distillation with toluene three times and then left under high vacuum (0.05 mbar) overnight. 120 mM phosphate buffer (10× PB) was prepared from sodium hydrogen phosphate (100 mM) and potassium dihydrogen phosphate (20 mM) diluted with

Millipore water. Millipore water was obtained from a Milli-Q Reference A + System (water was used at a resistivity of 18.2 MΩ cm^{-1} and total organic carbon of < 5 ppm). Deuterated solvents were obtained from Deutero. Deuterated toluene was purchased from Sigma Aldrich. For enzymatic degradation studies, a recombinant lipase immobilized on acrylic resin beads was used (Novozyme 435 ≥ 5000 U g^{-1}, recombinant, expressed in *Aspergillus niger*, from Sigma Aldrich). The solid support enables enzymatic polymer degradation studies both in organic (toluene) and aqueous environments. Dialysis was performed using Spectra/Por7 dialysis membranes with a molecular weight cut-off of 1000 g mol^{-1}. Sterile Dulbecco's PBS, cell culture medium and supplements were purchased from Thermo Fisher. The RAW-Blue reporter cell line, QUANTI-Blue reagent and Adifectin (CL347) were purchased from Invivogen and handled as recommended by the supplier.

2.2 Instrumentation

All ^{1}H-Nuclear Magnetic Resonance (NMR) spectra were recorded at room temperature on a Bruker 250 MHz, 300 MHz, 400 MHz or 600 MHz FT NMR spectrometer (Bruker Avance III 250, Bruker Avance III HD 300, Bruker Avance II 400, or Bruker Avance III 600). Chemical shifts (δ) are provided in parts per million relative to TMS. NMR spectra were processed with MestReNova 11.0.4 from Mestrelab Research. Samples were prepared in respective deuterated solvents and their signals referenced to the residual non-deuterated solvent signal. Integrals of proton signals of the block copolymer were normalized to the integral of the ethylene glycol units of mPEG, which were set to 194 protons (Fig. S13†). This relative number of protons has been determined from pure 2 kg mol^{-1} mPEG by ^{1}H-NMR referenced to its methyl end group. Diffusion Ordered Spectroscopy (DOSY) spectra were recorded at room temperature on a Bruker 400 MHz FT NMR spectrometer (Bruker Avance III HD 400) and processed using Bayesian DOSY Transformation (minimum: 1.00×10^{-8}; maximum: 1.00×10^{-4}; resolution factor: 1.00; repetition factor: 1; points in dimension: 64). The molecular weights of the polymers were determined using a size exclusion chromatography (SEC) set up composed of an Agilent Series 1100 with THF as the mobile phase (flow rate: 1 mL min^{-1}) equipped with an SDV column. Samples were run with toluene as an internal standard. All measurements were performed using an RI (Agilent G1362A) and UV (275 nm) detector. SEC data were analysed *via* WinGPC Unity using a PEG calibration (Polymer Standards Service Mainz). Dynamic light scattering (DLS) and zeta potential measurements were performed on a Zetasizer Nano ZS (Malvern Instruments Ltd, Malvern, U.K.) equipped with a HeNe laser (λ = 633 nm) and detected at a scattering angle of 173° at 25 °C. The obtained data were processed by cumulant fitting for *z*-average and PDI as well as by CONTIN fitting for particle size distribution. Unless otherwise stated, dust was removed from the sample prior to each measurement by filtration through a GHP syringe filter (0.45 μm pore size, Acrodisc). The zeta potential was measured by laser Doppler electrophoresis using folded capillary cells (Malvern, DTS 1070). The effective zeta potential was calculated using the Smoluchowski approximation. MALDI-ToF mass spectra were acquired on a rapiflexTM MALDI-ToF/ToF mass spectrometer from Bruker equipped with a 10 kHz scanning smartbeam 3D laser (Nd: YAG at 355 nm) and a 10 bit 5 GHz digitizer. Measurements were performed in positive reflector mode using DCTB (*trans*-2-[3-(4-*tert*-butylphenyl)-2-methyl-2-propenylidene]malononitrile) acid as a matrix. The data were processed with mMass and Origin 7.5/8.0. pH measurements were performed using a pH-measuring instrument (Seven Compact) manufactured by Mettler Toledo (standardized to pH 4, pH 7, pH 10). UV/Vis spectra were recorded on a Jasco V-630 spectrophotometer equipped with a Peltier thermostatted single cell holder (JASCO ETC-717) cooled by a water thermostat (A. Knüss Optronic V50) to guarantee measurement conditions at 25.0 °C.

2.3 Synthesis of a 2-methyl-1,3-dioxan-4-one (MDO) monomer

According to the literature,[17] the cyclic esteracetal-monomer 2-methyl-1,3-dioxan-4-one (MDO) was synthesized from racemic 2-methyldihydrofuran-3-one *via* Baeyer–Villiger oxidation. 77% *m*-CPBA (69.17 g; 309 mmol; 1.2 eq.) was dissolved in 600 mL methylene chloride (DCM), dried over MgSO$_4$, and filtered. With 100 mL of DCM, residual MgSO$_4$ was rinsed and filtered. The combined filtrates were transferred into a 2000 mL round bottom flask under a nitrogen atmosphere and cooled to 0 °C. 2-Methyltetrahydrofuran-3-one (25 mL; 257.2 mmol; 1 eq.) was added stepwise *via* a syringe over a time range of 30 minutes. The solution was then brought to room temperature and stirred for a further 21.5 h. The precipitated *meta*-chlorobenzoic acid was removed by repeated filtration at −78 °C. The volume of the solution was then concentrated to 60 mL under vacuum and filtered once more. The filtrate was washed with saturated sodium bicarbonate (8 × 20 mL) until no further carbon dioxide emission was evident. The aqueous fractions were extracted three times with DCM. The combined organic layers were washed with 10 mL of deionized water and subsequently dried over MgSO$_4$. Dichloromethane was removed by distillation. The crude oil was transferred into a 50 mL round bottom flask, dried over calcium hydride for 12 h at room temperature and subsequently distilled *via* short path distillation apparatus (56 °C, 5×10^{-2} mbar). The product was obtained as a colourless liquid (17.58 g; 151.40 mmol; 59%) and stored at −17 °C. The purified product was characterised by ^{1}H-, ^{13}C-, COSY- and HSQC-NMR spectroscopy. All spectra are provided in Fig. S1–S4.†

^{1}H-NMR (400 MHz, CDCl$_3$) δ [ppm] = 5.39 (q, *J* = 5.1, 1H; –O–C**H**(CH$_3$)–O–), 4.17 (ddd, *J* = 11.5, 8.2, 2.3, 1H; –C(O)–CH$_2$–C**H$_2$**–O–), 3.91 (ddd, *J* = 11.4, 10.7, 5.4, 1H; –C(O)–CH$_2$–C**H$_2$**–O–), 2.75 (ddd, *J* = 17.8, 10.7, 8.2, 1H; –C(O)–C**H$_2$**–CH$_2$–O–), 2.56 (ddd, *J* = 17.9, 5.4, 2.3, 1H; –C(O)–C**H$_2$**–CH$_2$–O–), 1.45 (d, *J* = 5.2, 3H; –O–CH(C**H$_3$**)–O–).

^{13}C-NMR (100 MHz, CDCl$_3$) δ [ppm] = 167.54 (–C(O)–); 101.17 (–O–CH(CH$_3$)–O–); 63.33 (–C(O)–CH$_2$–CH$_2$–O–); 29.93 (–C(O)–CH$_2$–CH$_2$–O–); 21.12 (–O–CH(CH$_3$)–O–).

2.4   Homopolymerisation of MDO

One day before polymerisation, pyrene butanol (35.15 mg; 0.13 mmol; 1/80 eq.) was weighed into a dried 5 mL Schlenk flask, dried by azeotropic distillation with toluene three times and further kept under high vacuum overnight. The polymerisation of MDO was carried out under a nitrogen atmosphere using dried glassware and a Teflon stir bar. MDO (1.0 mL; 10.25 mmol; 1 eq.) was added to pyrene butanol (volumetrically by using a 1 mL syringe). 0.27 mL of dichloroethane (DCE) was added as solvent. After complete solvation of all compounds, DPP was added from a prepared stock solution using a 1 mL syringe (200 µL of a 24.635 mM stock solution in DCE; 4.93 µmol; the amount corresponds to a ratio of 1/2080 DPP/MDO). Conversion of MDO was determined by ^{1}H-NMR. After 24 h, polymerisation was quenched using triethylamine (3.4 µL dissolved in 1 mL of DCM; 5 eq.) and stirred for 10 minutes. The crude product was subsequently purified by repeating precipitation three times in 40 mL of a THF/ n-hexane solution (1 : 9). The precipitate was isolated by centrifugation (4500 rpm, 20 min, 4 °C) and removal of the supernatant. The remaining pellet was dissolved in 1 mL of DCM and precipitated again. After drying under vacuum at room temperature, 237 mg of poly(pyrene butanol-PMDO) was obtained as a slightly yellowish, highly viscous liquid (19% yield relative to 100% of the monomer). The homopolymer was analysed by SEC, MALDI and ^{1}H-NMR as well as ^{13}C-NMR, COSY, HSQC and HMBC spectroscopy. All data are provided in Fig. S5–S12.†

SEC^{UV} (THF, PEG calibration): M_n = 2400 g mol^{-1}, PDI = 1.31.

^{1}H-NMR (400 MHz, CDCl$_3$) δ [ppm] = 8.33–7.79 (m, pyrene-H); 5.96 (q, J = 5.2, 1H; –O–CH(CH$_3$)–O–); 4.78–4.64 (m, pyrene–(CH$_2$)$_4$–O–CH(CH$_3$)–O–); 3.97–3.85 (m, 2H; –C(O)–CH$_2$–CHH–O–); 3.84–3.71 (m, 2H; –C(O)–CH$_2$–CHH–O–); 3.37 (t, J = 7.6 Hz; pyrene–(CH_2)–(CH$_2$)); 2.59 (m, 2H; –C(O)–CH_2–CH$_2$–O–); 2.09–2.00 (m; pyrene–(CH$_2$)–(CH_2)–(CH$_2$)); 1.99–1.89 (m; pyrene–(CH$_2$)$_2$–(CH_2)), 1.37 (d, J = 5.3, 3H; –O–CH(CH_3)–O–).

^{13}C NMR (100 MHz, CDCl$_3$) δ [ppm] = 170.95 (–C(O)–); 96.51 (–O–CH(CH$_3$)–O–); 64.42 (–C(O)–CH$_2$–CH$_2$–O–); 35.16 (–C(O)–CH$_2$–CH$_2$–O–); 20.76 (–O–CH(CH$_3$)–O–).

Polymerisation at 0 °C: yield 43%, SEC^{UV} (THF, PEG calibration): M_n = 3700 g mol^{-1}, PDI = 1.79.

2.5   Block copolymerisation of MDO onto mPEG

As an example, the synthesis of mPEG$_{48}$-b-P(MDO)$_{50}$ is described. One day before polymerisation, 129.36 mg (64.9 µmol; 1/158 eq.) mPEG was weighed into a 10 mL Schlenk tube equipped with a stir bar. For drying, 1 mL of toluene was added and the suspension was stirred for 10 min. Afterwards, the solution was frozen in liquid nitrogen and dried under reduced pressure (0.05 mbar). This procedure was repeated three times and the dried polymer was then kept at

0.05 mbar overnight. Into the prepared Schlenk tube equipped with a stir bar and dried mPEG, MDO was added volumetrically via a purged syringe (1 mL; 10.25 mmol 1 eq.). All compounds were dissolved without adding an additional solvent. Subsequently, 150 µL catalyst stock solution was added volumetrically (concentration: 32.846 mM stock solution in dichloromethane; 4.93 µmol; the amount corresponds to a ratio of 1/2080 DPP : MDO). Then, polymerisation was conducted at room temperature. Conversion of MDO was tracked by ^{1}H-NMR. After 23 h, further conversion was marginal (~1 monomer unit per hour) and, therefore, the polymerisation was quenched with triethylamine (1.5 eq.). (Note that in order to find an appropriate purification method, previous solubility experiments with pyrene butanol initiated homopolymers were conducted. They indicated that homopolymers are slightly soluble in diethyl ether, whereas mPEG precipitated well.) Therefore, the crude product was repetitively precipitated in Et$_2$O three times at −17 °C. Whereas the crude product of polymers with exceptionally shorter chain lengths precipitated directly, the longer chains precipitated only after cooling. For polymerisation conditions used at mPEG to monomer ratios of 95 and 126, the purified product was obtained as a colourless solid (yield: 31%), whereas for higher ratios the product was obtained as a viscous liquid. Summarized data of all reaction conditions applied to obtain mPEG$_{48}$-b-PMDO block copolymers are summarized in Table 1. Each polymer was further characterised by ^{1}H-NMR, ^{13}C-NMR, COSY, HMBC and HSQC and diffusion ordered spectroscopy (DOSY), as well as SEC and MALDI-ToF MS (compare Fig. S14–S30†).

SEC (THF, PEG calibration): M_n = 8800 g mol^{-1}, PDI = 1.65.

^{1}H-NMR: (400 MHz, CDCl$_3$) δ [ppm] = 5.96 (q, J = 5.3, 1H; –O–CH(CH$_3$)–O–); 4.77 (q, J = 5.3; mPEG–O–CH(CH$_3$)–O–); 3.75–3.85 (m, 1H; –C(O)–CH$_2$–CHH–O–); 3.98–3.85 (m, 1H; –C(O)–CH$_2$–CHH–O–); 3.64 (s, mPEG–(CH_2–CH_2–O–)); 3.38 (s; (–CH_3) methoxy-PEG), 2.67–2.50 (m, 4H; –C(O)–CH_2–CH$_2$–O–), 1.37 (d, J = 5.3, 3H; –O–CH(CH_3)–O–).

^{13}C-NMR: (100 MHz, CDCl$_3$) δ [ppm] = 170.91(–C(O)–); 96.44 (–O–CH(CH$_3$)–O–); 70.61 (mPEG–(CH$_2$–CH$_2$–O–), 64.36

Table 1   Result of MDO block copolymerisation onto mPEG

	χ_n^{targ}	Con. [%]	χ_n^{prod}	M_n^{prod} [g mol^{-1}]	M_n^{SEC} [g mol^{-1}]	$Đ^{SEC}$
mPEG$_{48}$-b-P(MDO)$_{15}$	95	44	15	3700	5000	1.46
mPEG$_{48}$-b-P(MDO)$_{23}$	126	44	23	4700	6000	1.57
mPEG$_{48}$-b-P(MDO)$_{50}$	158	55	50	7800	8800	1.65
mPEG$_{48}$-b-P(MDO)$_{71}$	190	54	71	10 200	10 300	1.48

χ_n^{targ}: Initial monomer to initiator (= mPEG) ratio; con.: monomer conversion during polymerisation determined by ^{1}H-NMR prior to polymer purification. χ_n^{prod}: monomer to initiator (= mPEG) composition of the purified polymer determined by ^{1}H-NMR using the resonance signals of the poly(esteracetal) proton and referencing them to the proton signals of the ethylene glycol units of PEG. M_n^{prod}: calculated molecular weight based on the χ_n^{prod} of the monomer and adding the molecular weight of the initiator (= 2 kDa mPEG). M_n^{SEC} and $Đ^{SEC}$: number average molecular weight and distribution determined by THF SEC using mPEG calibration.

(–C(O)–CH₂–*C*H₂–O–); 35.08 (–C(O)–*C*H₂–CH₂–O–); 20.71 (–O–CH(*C*H₃)–O–).

2.6 Self-assembly process of mPEG-*b*-poly(MDO)

(a) Solvent switch method. Approximately 10 mg of the diblock copolymer was dissolved in an appropriate volume of DMSO to target a concentration of 5 mg ml⁻¹. The solution was dialyzed against 1 L of 1× phosphate buffered-saline solution at a pH of 7.4. In the first attempt, dialysis was carried out over 4 days (the pH was checked to be neutral by using pH-indicator strips (MERCK) before and after dialysis). The solvent was exchanged every 24 hours. To prove preliminary degradation, the dialyzed solution was extracted with DCM and analysed *via* ¹H-NMR in CDCl₃ where only PEG as the degradation product could be found (acetaldehyde and 3-hydroxypropionic acid are water-soluble and could not be extracted). Therefore, for the subsequent micellar preparation, the dialysis time was reduced to 8 h and the solvent exchanged at 2 h intervals. Dialysis usually yielded a particle solution of approximately 6 mL. Particles were subsequently measured by DLS (Fig. S32 and Table S1†).

(b) Direct hydration technique. Approx. 4 mg of the polymer was weighed in a 5 mL Eppendorf tube, and an appropriate volume of 120 mM phosphate buffer (adjusted to a pH between 7.2 and 7.4) was added to target a concentration of 4 mg mL⁻¹. After ten minutes of shaking, the dissolution process was assisted by sonication for 15 min at 0 °C. Directly after preparation, micellar size distribution was analysed by DLS measurement at 25 °C (Fig. 3 and Fig. S33†).

(c) Critical micelle concentration (CMC) determination. The critical micelle concentration was determined by analysing the fluorescence intensities of solubilized pyrene's first and third vibronic band maxima I_1 and I_3 at 375 nm and 387 nm (Fig. S34 and S35†). Their ratio I_3/I_1 was plotted *versus* logarithmic molar polymer concentration (Fig. S36 and S37†) and linear extrapolations of the steady ratio and increase ratio were used to determine their intercept as the CMC. For this purpose, a 126.58 μM pyrene solution was first prepared by dissolving 25.6 mg pyrene in 100 ml acetonitrile. 82.8 μL of this solution was further diluted in 100 mL of acetonitrile to afford a 1 μM stock solution. Independently, three individual solutions of the same block copolymers at 1 mg mL⁻¹ were prepared in acetonitrile, too, and then sequentially diluted. For this purpose, 455 μL were serially diluted with 354 μL of acetonitrile. To each sample of the prepared dilution series, 200 μL of the 1 μM pyrene stock solution was added. Subsequently, all the organic solvent was removed *in vacuo* within approximately 2 h affording a polymer pyrene film. All subsequent steps were performed as fast as possible to minimize possible hydrolysis. 354 μL of 10× PB was added to each polymer pyrene film. The samples were sonicated for 30 min and repeatedly vortexed. Finally, 300 μL of each sample were pipetted into black 96 well plates and measured immediately using a microplate reader. Fluorescence emission was recorded at room temperature with an excitation wavelength of 333 nm and monitored from 360 to 450 nm (step size: 1 nm).

2.7 Dual pH-responsive degradation studies

(a) NMR degradation kinetics (Fig. S43 and S44†). Micelles were prepared *via* the dissolution method as described above. 8 mg mPEG₄₈-*b*-P(MDO)₁₅ was weighed in a 5 mL Eppendorf tube, and 1 mL of 120 mM phosphate buffer prepared in D₂O was added. The pD value was measured with a glass electrode standardized with aqueous buffer solutions at pH 4, 7 and 10. The pH-value can be approximated[19] using:

$$pH_{(buffer\ of\ D_2O)} = pH_{measured} - 0.41$$

Accordingly, the measured pD value of 7.5 correlates with a buffer with a pH of 7.1. After degradation, the pD dropped to a value of 7.0 which corresponds to a pH value of approx. 6.6.

After ten minutes of shaking, the dissolution process was assisted by sonication at 0 °C for 15 min. Subsequently, NMR analysis was conducted. The degradation was calculated by subtracting the relative amount of 3-hydroxypropanoic acid (determined by its proton signal referenced to the proton signal of the HO–C*H₂*– group) from the degree of polymerisation determined in CDCl₃.

(b) NMR analysis of micellar degradation products after exposure to acidic and basic conditions. For acidic degradation, micelles were prepared at a concentration of 8 mg mL⁻¹ in D₂O. To 1 mL of micellar solution, 50 μL of 1 M HCl or NaOH was added respectively and ¹H-NMR spectra were recorded 4 h after addition.

(c) SEC analysis of micelles after exposure to acidic and basic conditions. The degraded NMR samples from 2.7.b were analysed by THF-SEC. Before measurement, the pH was neutralized. The solution was diluted with THF to approx. 4 mg mL⁻¹, filtered and analysed.

(d) DLS analysis of micelles after exposure to acidic and basic conditions (Fig. 4A, Fig. S38 and S39†). To investigate the micellar response to poly(esteracetal) degradation, micelles were prepared *via* the direct dissolution method (as described in 2.6.b) and again analysed *via* DLS. For this purpose, the micelles were prepared in 120 mM phosphate buffer at pH 7.4. After preparation, the micelles were observed for approximately 2 h confirming normal particle formation and stability, and subsequently divided into three new cuvettes. To each of them either 10 vol% of 1 M HCL, phosphate buffer or 1 M NaOH was added. Subsequently, all probes were characterised by DLS over time at given time points (addition of 1 M HCl afforded pH 5.7, phosphate buffer remained neutral at pH 7.2 and addition of 1 M NaOH resulted in pH 10.8).

(e) Zeta potential analysis of micelles immediately after exposure to neutral, acidic and basic conditions (Fig. S40 and S54†). To verify the proposed mechanism of micelle behaviour in response to the change in pH, micelles were prepared (and loaded, respectively) as described *via* the direct hydration technique at a concentration of 4 mg mL⁻¹ in 5 mM HEPES buffer (at pH 7.14) and subsequently used for zeta potential analysis. The micelles were diluted threefold (300 μL of micellar solution with 600 μL of buffer), further acidified with 2 μL of 1 M HCl (affording a final pH ≈ 4), basified respectively with 3.5 μL

of 1 M NaOH (affording a final pH ≈ 10) and measured again. Data are given as mean ± standard deviation of three repeated measurements per sample.

2.8 Enzymatic degradation studies

(a) **Enzymatic NMR degradation kinetics in toluene (Fig. S45–S47†).** The non-self-assembled block copolymers could be degraded enzymatically by solid-supported lipase in organic solvent. For this purpose, 19.55 mg of mPEG$_{48}$-*b*-P(MDO)$_{71}$ was dissolved in 0.7 mL toluene-*d*$_8$ and 25 mg of Novozyme 435 was added. A sample without an enzyme served as a negative control. The degradation was determined based on the formation of acetaldehyde referenced to the aromatic resonance signal of residual toluene. The signal ratio of the intact polymer to toluene could be determined by NMR-analysis before enzyme addition.

(b) **Enzymatic NMR degradation kinetics in D$_2$O phosphate buffer (Fig. 5 and Fig. S48†).** The self-assembled block copolymer micelles could also be degraded enzymatically in aqueous solvent with solid-supported lipase. For this purpose, mPEG$_{48}$-*b*-P(MDO)$_{71}$ micelles were prepared at a concentration of approx. 15 mg mL^{-1} in 10× PB (prepared from D$_2$O with 1% dimethyl sulfone (DMS) as the internal standard; dimethyl sulfone was chosen as the reference, because the chemical shift is far apart from any relevant resonance signal; furthermore, it is highly hydrophilic, which minimizes potential interactions with the enzyme or micelles during degradation). 20 mg of Novozyme 435 per 1 mg of the polymer was added into the NMR tube. The resin floated on top of the sample and, therefore, did not interfere with the NMR measurement. At periodic intervals, NMR spectra were recorded and analysed (compare Fig. S48†).

(c) **Enzymatic DLS degradation kinetics (Fig. 5 and Fig. S49†).** Enzymatic micelle degradation could also be followed by DLS, as solid-supported lipase beads float on top of the aqueous medium inside the DLS cuvette. For this purpose, micelles were prepared as described by the direct hydration technique at a concentration of 4 mg mL^{-1}. Subsequently, 93.70 mg of Novozyme 435 were added to 900 μL of the micellar solution inside the cuvette and degradation was monitored *via* DLS. A sample without lipase served as the reference. Between each measuring time point, sealed samples were shaken on an orbital lab shaker.

2.9 Encapsulation and release of Nile Red into mPEG-*b*-poly(MDO) block copolymer micelles

(a) **Nile Red formulation.** In order to target a theoretical loading of 2.5 wt% of Nile Red, approx. 4 mg polymer was weighed in a 5 mL Eppendorf tube and dissolved in an appropriate volume of a Nile Red stock solution (*c* = 0.111 mg mL^{-1} in acetonitrile). Subsequently, the solvent was removed under vacuum over 2.5 h, resulting in a thin layer of Nile Red and mPEG-*b*-poly(MDO) covering the Eppendorf tube which enables a fast dissolution afterwards. 120 mM phosphate buffer was added targeting a polymer concentration of 4 mg mL^{-1}. Self-assembly and dye loading were assisted by

sonication at 0 °C for 30 minutes. After sonication, the particles were filtered *via* a GHP-filter with a pore size of 0.45 μm. The filtration step removed the precipitated dye, which was not encapsulated. After filtration, a pink solution without any visible precipitation was obtained. In analogy, reference samples were prepared that contained only the polymer or only Nile Red and served as blank probes (Fig. S50†). Directly after preparation, the micelles were analysed by DLS and UV/Vis spectroscopy.

(b) **Quantification of Nile Red loaded into mPEG-*b*-poly (MDO) block copolymer micelles.** Taking the particle self-absorbance due to micelle scattering into account, blank polymer micelle samples without a dye were subtracted from the UV/Vis absorption obtained for the loaded particles. The pH of the dye-loaded micellar solution was at 7.13. The measured absorbance spectra of micelles formulated with and without Nile Red are shown in Fig. 6. Nile Red loading could be quantified by comparison to an external calibration curve (Fig. S51 and S52†).

(c) **Nile Red release.** To investigate the kinetics of Nile Red release, the absorbance spectra of dye loaded micelles were recorded over time. Additionally, particle size distribution was recorded by DLS. For this purpose, micelles loaded with Nile Red were prepared as described above. For enzymatic degradation and dye release, 101.71 mg of Novozyme 435 were added to 1000 μL of loaded micelle solution inside the cuvette and degradation was monitored *via* both DLS and UV/Vis. A sample without an enzyme served as the reference. Between each measuring time point, sealed samples were shaken on the orbital lab shaker.

2.10 Formulation of TLR 7 agonist Adifectin loaded mPEG-*b*-poly(MDO) block copolymer micelles

For formulations with the amphiphilic polymers, 500 μg Adifectin was diluted with 500 μL ethanol targeting a concentration of 1 mg mL^{-1}. 128 μL of this stock solution was transferred each into two different 15 mL tubes, where one of them contained 4 mg of mPEG$_{48}$-*b*-PMDO$_{50}$. Both probes were subsequently freed from the solvent under reduced pressure, resulting in thin films covering the tube bottom. As described by the supplier, Adifectin itself was dissolved in ethanol, targeting a concentration of 10 μg μL^{-1} and vortexed. Once solubilized, the solution was diluted with 120 mM phosphate buffer to provide a 0.1 mM theoretical Adifectin solution and sonicated for 30 minutes. The formulation with the polymer was treated similarly. All samples were filtered through GHP-filters with a pore size of 0.45 μm. The prepared formulations were measured *via* DLS and the Adifectin concentration was quantified by UV/Vis spectroscopy.

2.11 Quantification of Adifectin loaded into mPEG-*b*-poly (MDO) block copolymer micelles

In analogy to the quantification of Nile Red loading, the Adifectin concentration was determined by comparison to an external standard curve in ethanol (Fig. S61A + B†). Adifectin shows a peak maximum at 297 nm. The scattering absorbance

of unloaded particles was subtracted from the UV/Vis absorption value obtained for the loaded particles (Fig. S61C†).

2.12 Raw Blue macrophage cell culturing

RAW-Blue macrophages were cultured in Dulbecco's modified Eagle's medium (DMEM) supplemented with 10% fetal bovine serum, 1% penicillin/streptomycin, 0.02% Normocin and 0.01% Zeocin at 37 °C with 5% CO_2 saturation.

2.13 TLR 7 stimulation assay

Adifectin TLR receptor stimulation followed by NF-kB/AP-1 activation (detected by the secretion of embryonic alkaline phosphatase) was performed on RAW-Blue cells as recommended by the manufacturer (InvivoGen). RAW-Blue cells were seeded into 96-well plates at a density of 90 000 cells per well in 180 μL culture medium. The cells adhered overnight and then they were treated in each well with 20 μL of the sample at given Adifectin concentrations (listed in Table S2†). After stimulation for 16 h, 50 μL of the supernatant from each well was collected and probed for secreted embryonic alkaline phosphatase (SEAP) using the QUANTI-Blue assay (InvivoGen). 150 μL QUANTI-Blue was added to each sample and incubated at 37 °C. Secretion of embryonic alkaline phosphatase levels were determined by measuring the optical density at 650 nm using the microplate reader. Activity was determined by an increase in the optical density relative to the negative control treated with PBS. The TLR 7/8 agonist 1-(4-(aminomethyl)benzyl)-2-butyl-1*H*-imidazo[4,5-*c*]quinolin-4-amine (IMDQ) served as a positive control, as used in previous experiments.[12–14] A minimal interference between the 120 mM phosphate buffer and the SEAP assay was observed, due to an increased phosphate concentration. Therefore, the obtained results were corrected based on the contribution of the 120 mM phosphate buffer blank and the PBS blank. All experiments were conducted in quadruplicate ($n = 4$).

2.14 Cell viability assay

50 μL of 3-(4,5-dimethylthiazol-2-yl)-2,5-diphenyltetrazolium bromide (MTT) (0.5 mg mL^{-1} in PBS) was added to the RAW-Blue macrophages that were treated with the corresponding samples at given Adifectin/polymer concentrations. After MTT incubation for 3 h, the formazan crystals formed were dissolved by the addition of 100 μL of 10% m/v SDS/0.01 M HCl and incubated overnight at 37 °C. Quantification was done by measuring the absorbance at 570 nm using the microplate reader. Cell viability was calculated in relation to positive (blank PBS, referred to as 100% viability) and negative (10% DMSO, referred to as 0% viability) control samples. All experiments were conducted in quadruplicate ($n = 4$).

3. Results and discussion

Among different classes of amphiphilic polymers used for drug delivery, only a few guarantee full fragmentation into small molecules upon exposure to external stimuli. Poly(estera-cetal)s can provide such degradation features towards variation in pH both below and above physiological values. While the ester group in the backbone is prone to basic hydrolysis or enzymatic degradation, the additional acetal group enables acid triggered depolymerisation occurring in tumour microenvironments and their draining lymph nodes, as well as intracellularly inside endolysosomes. To the best of our knowledge, polymerising hydrophobic poly(esteracetal)s onto hydrophilic polymers providing amphiphilic poly(esteracetal)s has not been reported before and will be examined in this work with respect to applications in immunodrug delivery.

3.1 MDO monomer synthesis

According to the literature,[17] the cyclic esteracetal-monomer 2-methyl-1,3-dioxan-4-one (MDO) was synthesized from racemic 2-methyldihydrofuran-3-one *via* Baeyer–Villiger oxidation. The purified product was dried over calcium hydride and distilled under vacuum. The compound was obtained as a colourless liquid with a yield of 59%. The structure of the product could be validated by ^{1}H-NMR, ^{13}C-NMR, COSY- and HSQC-NMR spectroscopy and the results are shown in Fig. S1–S4.† As we observed that MDO slowly degraded over time into 3-hydroxypropanoic acid and acetaldehyde, it was stored at −18 °C and always distilled freshly prior to use.

3.2 Homopolymerisation of poly(MDO)

Hillmyer *et al.* have previously evaluated the ring-opening homopolymerisation of MDO using diphenyl phosphoric acid (DPP) as an organic catalyst.[18] Attributed to low thermodynamic driving forces for ring-opening of MDO and achieve equilibrium conditions during polymerisation, reaction conditions at high dilutions prohibit high monomer conversion. Therefore, Hillmyer *et al.* performed homopolymerisations in the bulk.[18,20] These conditions seem to be primarily difficult for later block copolymerisations. Accordingly, MDO polymerisation conditions are required which take into account both solubility and dilution by a macroinitiator.

To address this question, we initially tested polymerisation at 7 M monomer dilution using pyrene butanol as the initiator (compared to ~10 M in the bulk).[17] Polymer purification was performed as described by Hillmyer *et al. via* precipitation in hexane THF (9 : 1) and subsequent drying under reduced pressure at room temperature. Poly(pyrene butanol-P(MDO)) was characterised by NMR, SEC and MALDI-ToF MS (Fig. S5–S12†). ^{1}H-NMR analysis confirmed successful ring-opening of the cyclic monomer. The characteristic quartet resonance signal at 5.96 ppm verified the incorporation of poly(esteracetal)s into the polymer backbone.[17,18] Signals corresponding to the pyrene butanol end group were found in the ^{1}H-NMR spectrum, too (with the assistance of the ^{1}H-NMR derived COSY-NMR spectrum, because some relevant pyrene butanol signals were partially covered by other resonance signals – compare Fig. S7†).

By size exclusion chromatography (SEC) we observed reasonably narrow dispersities and in the elugrams UV absorption emerged nearly simultaneously with the refractive index

(Fig. S11†), which confirmed that pyrene butanol was present as an end group on the poly(esteracetal)s (note that poly(ester-acetal)s themselves are not UV active).

In accordance with that, we could find intact MDO monomer repeating units (116 g mol⁻¹) by MALDI ToF mass spectrometry. A comparison with simulated mass peaks supported successful integration of one pyrene butanol as an end group onto mostly multimeric esteracetal moieties and only minor (one or two) integration of ester units into the backbone (Fig. S12†). Interestingly, comparatively small mass peaks matched the formation of cyclic homopolymers without any pyrene butanol end group. As rationalized by others, these concurring side reactions can hardly be suppressed completely under the applied reaction conditions.[18,21] MDO can polymerise after self-initiation *via* an activated chain end mechanism into either homopolymers with an enol ester end group or a cyclized product. Based on their similar molecular weights MALDI-ToF MS cannot differentiate between polymers terminated by an enol ester end group and cyclized polymers. In fact, only a minor formation of such a product was found in the mass spectra (Fig. S12†); however, by ¹H-NMR spectroscopy no enol ester signals were observed. Instead, only esteracetal protons of the cyclized side products were detectable (the signals overlap with the pyrene butanol end group derived acetal signal – Fig. S5 and S6†).

Taken together, the combined results from ¹H-NMR, SEC and MALDI-ToF MS analyses confirmed that the synthesis of pyrene butanol initiated poly(MDO) can be achieved under slightly diluted conditions in the presence of solvents. For equilibrium polymerisation conditions, the overall observed conversion should decrease at higher dilution compared to bulk polymerisation. Alternatively, reduced temperatures would thermodynamically favour higher conversions. We, therefore, performed also polymerisations at 0 °C, and indeed higher conversions could be found at longer reaction times; yet, we also observed broader molecular weight distribution (PDI increased from 1.31 to 1.79). We attribute this to lower viscosities at these temperatures that might further be affected by the presence of polymers. The latter would be more relevant for block copolymerisations using mPEG macroinitiators.

To conclude, polymerisations at room temperature and monomer dilutions at 7 M seem to result in acceptable product formation and were, therefore, applied in the following block copolymerisation reactions.

3.3 Block copolymerisation of mPEG-*b*-poly(MDO)

A variety of amphiphilic block copolymers were synthesized by polymerising MDO onto mPEG₄₈ (2000 g mol⁻¹). mPEG is commonly used as a hydrophilic, non-toxic coating for nanomedicines, because its stealth-like properties prevent opsonisation and plasma protein binding, increase colloidal stability and prolong circulation half-life.[22] For polymerising MDO onto it, we applied the previous conditions of homopolymerisation. With respect to high monomer concentrations for MDO ring-opening, the diluting effect of the macroinitiator mPEG needs to be taken into account. We, therefore, adapted

the solvent volume targeting a concentration between 7 M and 8 M (the mPEG-density was assumed to contribute only by its solid density). It was necessary to dissolve the macroinitiator-mPEG first in the monomer to ensure sufficient mixing before the DPP catalyst was added (pre-dissolved in the remaining solvent).

By varying the monomer to initiator ratio, we could target different poly(MDO) block lengths. Conversion of MDO was tracked by ¹H-NMR. After 23 h, an equilibrium was reached (further conversion was marginal) and, consequently, the polymerisation was quenched with triethylamine. In order to find an appropriate purification method, previously conducted solubility experiments with pyrene butanol initiated homopolymers indicated that they are slightly soluble in diethyl ether, whereas mPEG does precipitate well. Therefore, the crude product was subsequently precipitated in Et₂O three times at −17 °C. We obtained different PMDO block lengths at polymerisation degrees between 15 and 71 relative to the mPEG units. The obtained results are summarized in Table 1.

¹H-, ¹³C- and 2D-NMR analyses confirmed the successful formation of mPEG-poly(esteracetal) block copolymers in all cases and the absence of major impurities. As an example, the ¹H-NMR spectrum of mPEG₄₈-*b*-P(MDO)₅₀ is shown in Fig. 2A
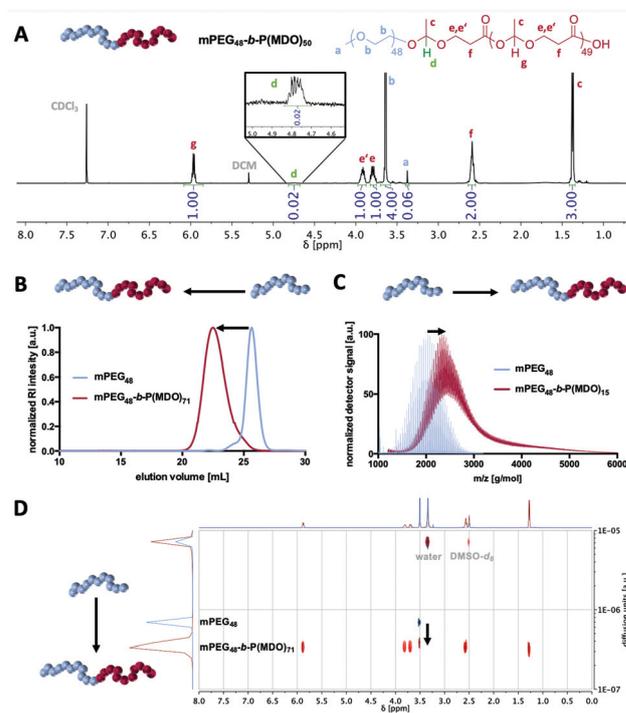

Fig. 2 Characterisation of amphiphilic mPEG-*b*-PMDO block copolymers. A: ¹H NMR (400 MHz) of mPEG₄₈-*b*-PMDO₅₀ in CDCl₃. Resonance signals of the macroinitiator and the PMDO block as well as one single acetal proton between the PEG block and the first MDO monomer unit are annotated. B: SEC elugram of the mPEG₄₈-*b*-PMDO₇₁ block copolymer (red) and the mPEG₄₈ macro-initiator (blue). C: MALDI-ToF mass spectra of the mPEG₄₈-*b*-PMDO₁₅ block copolymer (red) and the mPEG₄₈ macroinitiator (blue). D: ¹H-derived DOSY spectra (400 MHz) of the mPEG₄₈-*b*-PMDO₇₁ block copolymer (red) and the mPEG₄₈ macroinitiator (blue).

while all remaining spectra can be found in the ESI (Fig. S14–S29,† the degree of polymerisation of the MDO block was determined based on the integral of the poly(esteracetal) groups referenced to the ethylene glycol units of mPEG). Notably, the presence of exactly one single acetal proton signal can further be observed derived from the ring-opening of the first MDO monomer unit by mPEG.

We carefully used additional characterisation methods beyond ^{1}H-NMR spectroscopy to prove successful block copolymer formation, as displayed in Fig. 2B–D. By size exclusion chromatography (SEC) and by DOSY NMR and MALDI-ToF MS analyses a distinct shift to higher molecular weights/slower diffusion species was achieved for all block copolymers, while signals of the remaining unmodified mPEG macroinitiator were generally absent (Fig. S16, S19, S22 and S25†).

In the MALDI-ToF mass spectra, repetitive MDO (116 g mol^{-1}) and ethylene glycol (44 g mol^{-1}) units can be found (Fig. S15, S18, S21 and S24†). By detailed analysis and comparison with simulated mass signals (Fig. S30†), several mass peaks can be annotated to block copolymer species and not be explained by non-modified mPEG or self-initiated P(MDO) homopolymers.

Taken together, these results clearly demonstrate that poly(MDO)s can be attached with varying molecular weights onto mPEG and the resulting amphiphilic poly(esteracetal) block copolymers are further investigated for their self-assembly and drug encapsulation performance.

3.4 Block copolymer self-assembly

Generally, nanoparticles within a size range between 10 nm and 100 nm are considered as ideal drug carrier systems for several purposes including lymph node targeting after subcutaneous injection.[13,23,24] For the latter, such particles would be large enough to prevent fast clearance by the bloodstream, but still small enough to provide sufficient diffusion through the water channels of the interstitium into the lymphatic system.

Therefore, we investigated the influence of the hydrophobic chain length of the mPEG-b-poly(MDO) block copolymers on their self-assembly behaviour in aqueous media. Note that poly(MDO) homopolymers alone could not be solubilised in water after extensive mixing (Fig. S31†). Thus, it was at first intended to prepare block copolymer micelles via a simple dialysis-derived solvent switch method, which is most commonly used for micelle preparation.[25,26] For this purpose, the block copolymers were dissolved in DMSO and dialyzed against water. Subsequent DLS measurement revealed aggregates with a size of approximately 100 nm (Fig. S32†). However, an unusually low scattering intensity implied preliminary degradation during the self-assembly process. In fact, when dialysis was performed for several days, no particles could be detected anymore and ^{1}H-NMR proved polymer degradation to solely mPEG (Fig. S32†).

In this respect, an alternative preparation method had to be applied to access block copolymer micelles rapidly. It has been reported that for amphiphilic block copolymers with relatively

low glass temperatures (T_g) for their hydrophobic blocks, micelles can be prepared via direct hydration.[25] Interestingly, poly(MDO) homopolymers seem to provide such low T_g as the isolated polymer behaving like a highly viscous liquid (according to the literature,[17] the T_g is around −30 °C). A direct hydration without the assistance of further organic solvents is a fast preparation method and would reduce preliminary hydrolysis as the hydrophobic domains are immediately forced into self-assembled and shielded structures in the aqueous environment. Thus, they would instantaneously be protected from hydrolysis compared to solvent exchange methods, where mixtures of organic and aqueous solvents are present during dialysis and cannot shield the hydrophobic block from degradation immediately.

For the direct hydration formulation, 120 mM phosphate buffer was directly added to the block copolymers and the subsequent dissolution and self-assembly process was assisted by ultrasonication at 0 °C. Indeed, DLS measurements proved the formation of micelles at different sizes depending on the length of the hydrophobic block. As shown in Fig. 3, micellar sizes could be varied from 26 nm to 141 nm depending on the molecular weight of the P(MDO) block. Moreover, the reproducibility of the direct hydration formulation method could further be validated by preparing micelles from mPEG$_{48}$-b-P(MDO)$_{50}$ independently three times. Subsequent DLS measurement always indicated almost identical micelles with similar sizes and distributions (Fig. S33†).

In addition, the critical micelle concentration (CMC) was determined for mPEG$_{48}$-b-P(MDO)$_{15}$ and mPEG$_{48}$-b-P(MDO)$_{50}$ via pyrene fluorescence spectroscopy in order to compare the influence of the hydrophobic P(MDO) block on the self-assembly behavior. The intensities of pyrene's first and third vibronic band maxima I_1 and I_3 at 375 nm and 387 nm varied depending on the molar block copolymer concentration (Fig. S34 and S35†). The critical micelle concentration (CMC) was then estimated by plotting the ratio I_3/I_1 $versus$ logarithmic molar polymer concentration (Fig. S36 and S37†). Thereby, for the mPEG$_{48}$-b-P(MDO)$_{50}$ block copolymer with a 3.3-fold larger P(MDO) block, a 3.3-fold lower CMC could be determined,
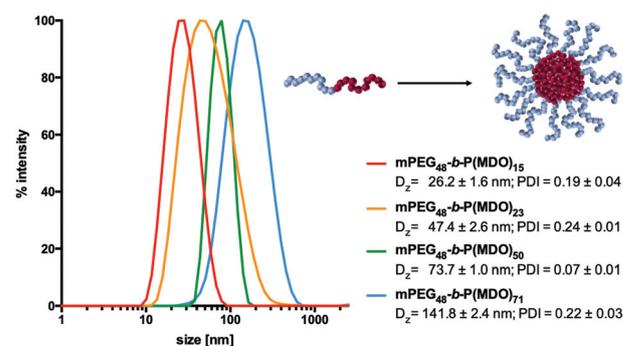

Fig. 3 Intensity size distribution plot of polymeric micelles prepared from mPEG-b-P(MDO) block copolymers of different hydrophobic block lengths via a direct hydration technique.

which confirms that block copolymer self-assembly is triggered by the P(MDO) block in aqueous media.

Altogether, the synthesized amphiphilic mPEG-*b*-P(MDO) block copolymers show an attractive self-assembling behaviour and their resulting micellar size ranges are ideal for drug delivery purposes including passive lymph node delivery.[13,23]

3.5 Dual pH-responsive degradation

To generally verify the dual pH-responsive degradation profile of mPEG-*b*-poly(MDO) block copolymers, micelles were exposed to acidic and basic conditions in aqueous media and analysed *via* ^{1}H-NMR. For this purpose, micelles were prepared from mPEG$_{48}$-*b*-poly(MDO)$_{15}$ in D$_2$O. Under these conditions, the poly(MDO) block is not observable (Fig. 4B). However, 30 min after the addition of 5 vol% 1 M HCl or NaOH, more than 80% of the degradation products appeared in the ^{1}H-NMR spectra. A measurement after 4 hours showed com-

plete degradation, as shown in Fig. 4B. The micelles degrade into acetaldehyde, 3-hydroxypropanoic acid and mPEG$_{48}$. Note that acetaldehyde can afterwards either form a hydrate under acidic conditions or isomerize to its enol and react further by aldol condensation under basic conditions (Fig. 4B). All of these degradation products could be found in the ^{1}H-NMR spectra. In analogy to these observations, also the elugram of subsequent SEC measurements proved complete poly(MDO) block degradation to the remaining hydrophilic mPEG-block, as shown in Fig. S42.†

To investigate the degradation of the block copolymers on the micellar self-assembly behaviour, intact micelles were prepared in 120 mM phosphate buffer and monitored by DLS under acidic, neutral and basic conditions. After the integrity of the micelles was monitored under neutral conditions for up to two hours, they were treated with either 10 vol% of 1 M HCL, phosphate buffer or 1 M NaOH, respectively. Thereby,
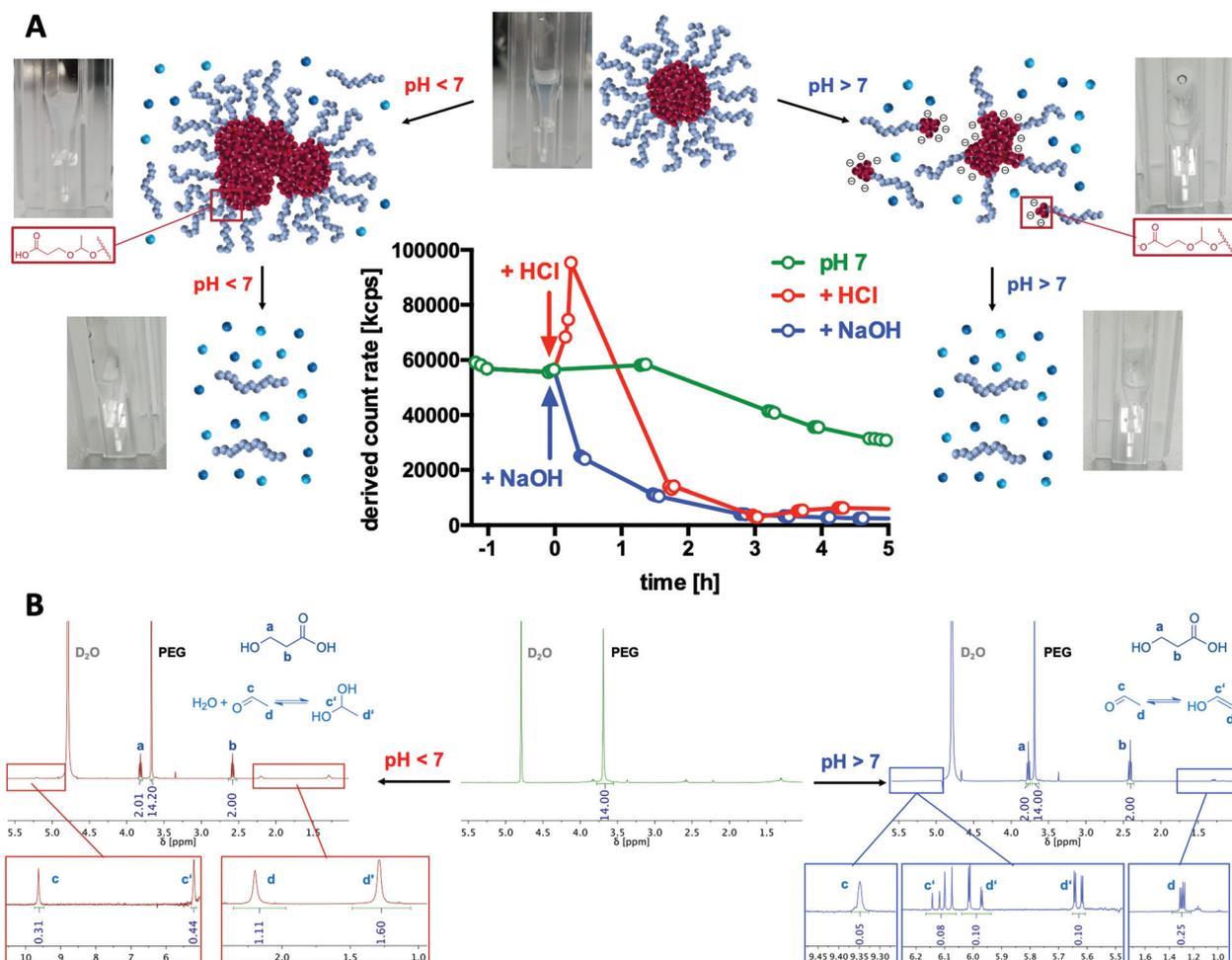

Fig. 4 Dual pH-responsive degradation profile of mPEG-*b*-P(MDO) derived block copolymer micelles. (A) Scattering intensity observed using DLS (derived count rate) over time under acidic (pH = 5.7), neutral (pH = 7.2), and basic conditions (pH = 10.8) with photographs of the corresponding samples inside the cuvette and a proposed mechanism explaining the degradation and self-assembly behaviour. (B) ^{1}H-NMR analysis (400 MHz) of micelles under neutral conditions and after acidic and basic degradation. Due to the suppressed molecular motion of the P(MDO) block inside the micellar core, the corresponding proton signals are diminished. Under acidic and basic conditions, micelles degrade into 3-hydroxypropionic acid and acetaldehyde (note that acetaldehyde can form hydrates under acidic conditions or further isomerize to enols and form aldol adducts at basic pH).

the pH dropped to 5.7, remained constant at 7.2 or increased to 10.8. For the various pH values, a significant drop in the scattering intensity was found after 2 hours indicating that micelle degradation under both acidic and basic conditions was tremendously accelerated (Fig. 4A).

Interestingly, further analyses revealed that under acidic conditions micelles first formed micrometre-sized aggregates, as shown by an increase in scattering intensity (Fig. 4A). Corresponding DLS-derived size distribution curves can be found in Fig. S38.† This responsive aggregation was also visible to the naked eye due to the massive increase in turbidity, yet, it disappeared after 2 h completely. We hypothesize that this aggregation might be a consequence of preliminary hydrolysis of the stabilising PEG units at the interface between the hydrophobic cores and their hydrophilic coronas. Consequently, the hydrophobic domains are not sterically shielded anymore and, therefore, aggregate into large particles. To support this hypothesis, we performed zeta potential measurements immediately after lowering the pH and found an increase from slightly negative (-13 ± 6 mV) to neutral (-3 ± 7 mV) zeta potential values corresponding to a charge neutralization by protonation of the carboxylate groups formed (Fig. S40†). We schematically depict this behaviour in Fig. 4A.

In contrast, under basic conditions, micelles did not aggregate but gradually fragmentized into smaller particles, as found from a gradual decrease in the count rate (Fig. 4A) and from the monitored size distribution plots (Fig. S35†). Presumably, under basic conditions, the particles are slightly charged by the deprotonated carboxylic end groups, which prevent aggregation due to charge repulsion. This could again be confirmed by zeta potential measurements directly after increasing the pH, where slightly negative zeta potential values (-13 ± 6 mV) further dropped to more negative values (-25 ± 6 mV) which contributed to the colloidal stability of the degradation fragments formed in aqueous media (Fig. S40†).

According to preliminary published data suggesting acidic compartments to be present in compartments of lymph nodes,[15] we want to pinpoint that such pH-responsive aggregation behaviour might be a promising strategy for tissue-selective particle trapping.

Micelle stability was also monitored over time under neutral conditions. In Fig. 4A, a gradual decrease in the light scattering count rate is observed for mPEG-*b*-P(MDO) block copolymers, too, although in a slower fashion. Retained micellar breakdown is desirable because degradation into hydrophilic small molecules with reasonably low molecular weight is expected to enable easy renal carrier clearance from the body, preventing long-term accumulation.[27]

Comparison of micelles derived from different P(MDO) block lengths showed that those with the shortest P(MDO) content were already degraded in a few hours (Fig. S41†). We were able to track their degradation kinetics *via* ^{1}H-NMR in phosphate-buffered D_2O, too, as illustrated in Fig. S43 and S44.† Interestingly, the kinetics perfectly matched the timeframes of disassembly observed by DLS as shown in Fig. S41.† An increased particle stability, however, was confirmed for

block copolymers with increasing hydrophobic block lengths (Fig. S41†). Micelles from mPEG$_{48}$-*b*-P(MDO)$_{50}$ exhibited a reasonable stability and combined with their size below 100 nm they were considered most promising for further delivery purposes.

3.6 Enzymatic degradation

Acid hydrolysis conditions can physiologically occur either intracellularly (*e.g.* in endolysosomes at pH levels of up to 5) or extracellularly (*e.g.* in immunosuppressive tumour microenvironments or lymph nodes[27]). Basic pH levels, however, are generally not reached under physiological conditions; yet, many hydrolytic esterase enzymes apply base-catalysed mechanisms to cleave ester bonds. Consequently, we studied poly(MDO) degradation behaviour in the presence of esterases and chose lipase as an enzyme with high ester-cleaving activity at hydrophilic–hydrophobic interfaces.

In first trials, the enzymatic degradation was tested on non-self-assembling single mPEG-*b*-P(MDO) poly(esteracetal) block copolymers. Yet, this could only be conducted in the presence of organic solvents (Fig. S45†). For this purpose, a recombinant lipase immobilized on acrylic resin beads was used (Novozyme 435), which facilitates ester cleavage in both organic (toluene) and aqueous environments according to the manufacturer. Block copolymer degradation experiments were performed in toluene-d_8 in order to monitor the formation of small molecular degradation products by ^{1}H-NMR over time (Fig. S46†). As control samples, mPEG-*b*-P(MDO) block copolymers were analysed in toluene-d_8 without an enzyme, too, and they proved high polymer stability in organic media over 1 week (Fig. S47†). In the presence of lipase, however, gradual P(MDO) block degradation was observed from an increase in the formation of acetaldehyde coupled with a decrease of the polymeric esteracetal resonance signal (Fig. S46†). According to the low amount of water present in the toluene reaction mixture, polymer degradation was not complete and reached around 50% after 90 h (Fig. S47†). These results motivated us to perform further lipase degradation experiments also in buffered aqueous media (Fig. 5).

For this purpose, mPEG-*b*-P(MDO)$_{71}$ micelles were prepared in H_2O or D_2O (supplemented with 120 mM phosphate at pH 7) by the direct hydration method (Fig. 5A). After the addition of lipase Novozyme 435, accelerated release of 3-hydroxypropionic acid and acetaldehyde (and its hydrate form, respectively) could be detected by ^{1}H-NMR (Fig. 5B). Kinetic monitoring of the ^{1}H-NMR samples over time revealed that already within the first 1.5 h almost all P(MDO) was hydrolysed into its small molecular degradation products (Fig. 5C), while in the control sample without an enzyme these hydrolysis products could be found gradually (after 90 h the expected amount of degradation products could be observed, Fig. S48†).

These findings could be well correlated with the scattering intensities observed during DLS kinetic experiments in the presence of lipase. The count rates of the formulated mPEG-*b*-P(MDO)$_{71}$ micelles dropped within 2 h dramatically (Fig. 5D), while a gradual decrease was found for the control samples
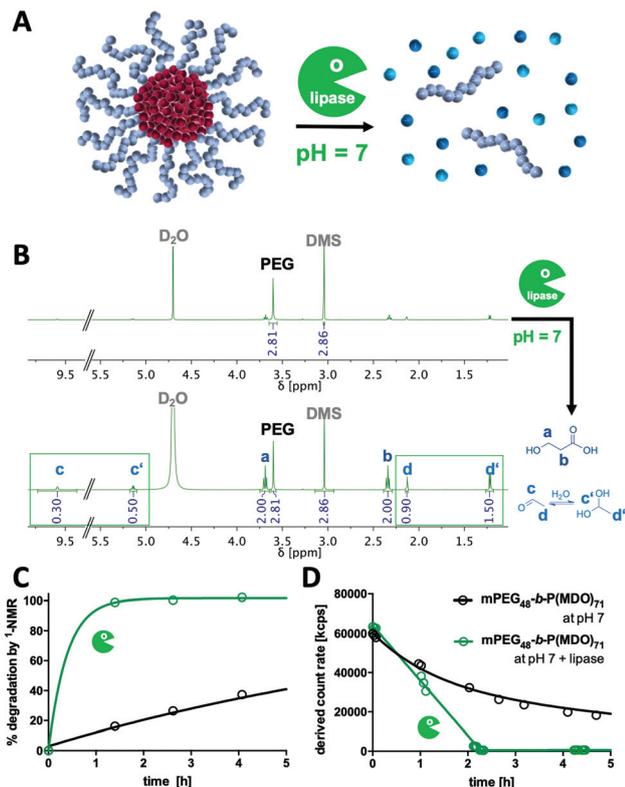
Fig. 5 Lipase-catalysed enzymatic degradation profile of mPEG-*b*-P(MDO)$_{71}$ derived block copolymer micelles. (A) Schematic representation of lipase mediated micelle degradation of the hydrophobic P(MDO) block at pH 7. (B) ^{1}H-NMR analysis (400 MHz) of micelles under neutral conditions before and after the addition of lipase. Due to the suppressed molecular motion of the P(MDO) block inside the micellar core, the corresponding polymeric proton signals are first diminished; however, upon addition of lipase, micelles release 3-hydroxypropionic acid and acetaldehyde (or its hydrate form, respectively). (C) ^{1}H-NMR kinetic analysis of accelerated enzymatic P(MDO) degradation for mPEG$_{48}$-*b*-P(MDO)$_{71}$ block copolymer micelles over time in 120 mM phosphate buffer. (D) Scattering intensity kinetics observed using DLS (derived count rate) of accelerated lipase-mediated P(MDO) degradation of mPEG$_{48}$-*b*-P(MDO)$_{71}$ block copolymer micelles over time in 120 mM phosphate buffer.

only over a longer time frame (Fig. S49†). Interestingly, in analogy to the DLS kinetic experiments in the presence of NaOH, no increase in turbidity or scattering intensity was found during lipase-mediated degradation in contrast to the acid-catalysed degradation process at lower pH (Fig. 4A). Consequently, lipase-mediated P(MDO) degradation probably follows a similar base-catalysed hydrolysis process, as hypothesized in Fig. 4A (right), and confirms the unique dual pH-responsive versatility of mPEG-*b*-P(MDO)-based micelles for drug delivery purposes.

3.7 Loading and release studies

Ideal micellar-drug delivery systems should be able to encapsulate drugs inside their cores and release them upon desired stimuli that arise at their targeted site of action. To investigate the encapsulation and release performance of mPEG$_{48}$-*b*-P(MDO)$_{50}$ derived block copolymer micelles, Nile Red as a hydrophobic and water-insoluble dye was encapsulated to mimic hydrophobic drug model compounds (Fig. 6). Interestingly, the fraction of encapsulated Nile Red can be quantified by UV/Vis spectroscopy, while non-encapsulated Nile Red precipitates in water (solubility < 1 µg mL^{-1}) and can be filtered off easily (Fig. S50 and S51†).[28–31]

Micelles formulated with Nile Red were prepared *via* an adapted direct hydration method targeting a theoretical loading of 2.5 wt% of Nile Red. For this purpose, a polymer film containing Nile Red was first prepared from organic solvent and evaporated prior to direct hydration of the mixture. After sonication, the particles were filtered in order to remove the non-encapsulated, precipitated dye (a schematic representation of the preparation is shown in Fig. S50†). After filtration, pink solutions without any visible precipitation were obtained. In comparison, applying the same procedure to pure Nile Red but lacking the amphiphilic polymer led to a clear colourless solution which also showed no characteristic absorbance band for Nile Red (compare Fig. 6B and Fig. S50†). The loaded micelles were subsequently analysed by DLS and an increase in size confirmed successful dye encapsulation (Fig. 6C).

Moreover, Nile Red loading could be quantified by UV/Vis spectroscopy applying an external Nile Red standard curve determined in ethanol (Fig. S51 and S52†). Pure polymer micelles served as a reference for absorbance due to particle scattering (Fig. 6D). Based on the observed findings, a dye loading efficiency of 19% was achieved for the mPEG$_{48}$-*b*-P(MDO)$_{50}$ derived block copolymer micelles, and it corresponds to a dye loading of 0.5 wt%. Depending on the length of the P(MDO) block, drug loading and encapsulation efficiency could also be varied (Fig. S53†). For mPEG$_{48}$-*b*-P(MDO)$_{50}$, only 3.8% of the dye could be encapsulated affording a 0.1 wt% dye load, while for the larger mPEG$_{48}$-*b*-P(MDO)$_{71}$ polymers with higher hydrophobic to hydrophilic ratios, 36% of the dye was formulated into the corresponding micelles affording a 0.9 wt% dye load, as determined by UV/Vis spectroscopy (Fig. S53†).

In addition, zeta potential measurements were conducted showing that dye loading hardly affected the zeta potential of the Nile Red loaded mPEG$_{48}$-*b*-P(MDO) micelles. Unloaded micelles provided a slightly negative zeta potential of −13 ± 6 mV that barely increased upon dye loading to −10 ± 10 mV, which is not significantly different. This behaviour can be explained by the rather low Nile Red loading below 1 wt%.

Subsequent drug release measurements were conducted and they correspond to previous particle degradation (compare Fig. 4A and 5A). After decreasing the pH by addition of HCl, Nile Red loaded micelles again started to aggregate instantaneously, whereas under basic conditions aggregation was not observed (compare Fig. S55†). Consequently, under acidic conditions, DLS studies cannot be performed properly to correlate them with Nile Red release. We, therefore, followed the process visually with the naked eye (Fig. S56†) and observed a
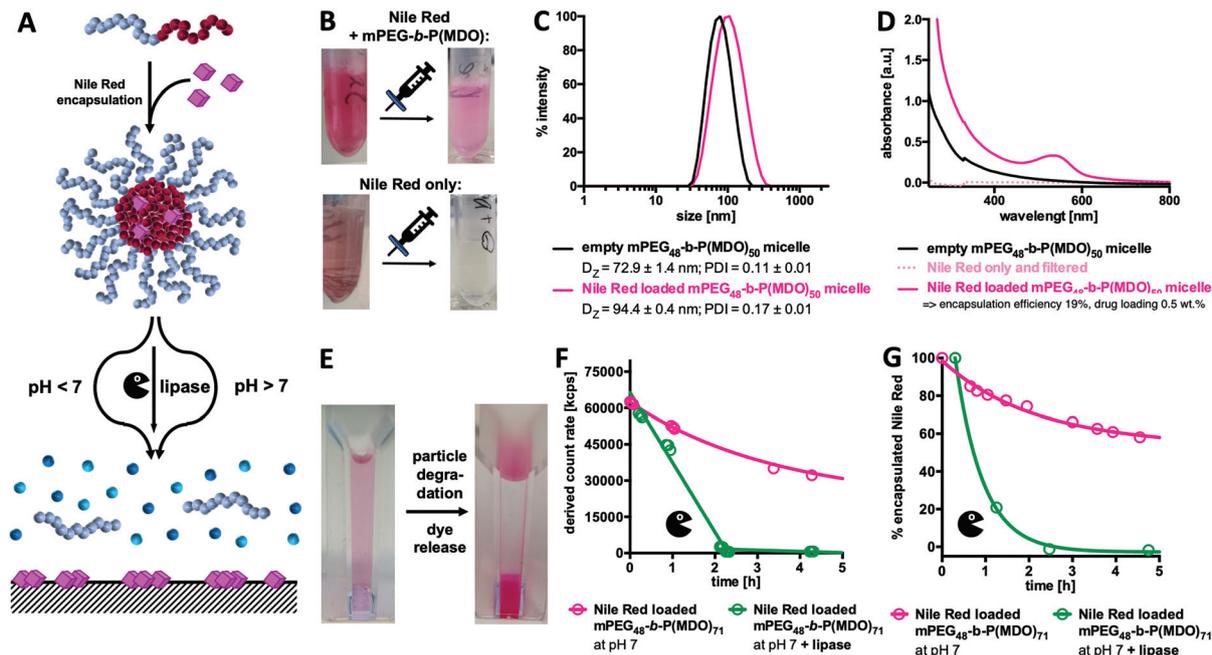
Fig. 6 Nile Red formulated into mPEG$_{48}$-b-P(MDO)$_{50}$ micelles. (A) Schematic representation of Nile Red loading and release. Under acidic and basic conditions, micellar degradation is highly accelerated. Upon degradation, Nile Red is expected to be released and precipitate. (B) Nile Red formulated with and without the polymer. Pictures are shown before and after filtration (450 μm). Whereas Nile Red formulated with the polymer is stabilized in solution, Nile Red was solely removed by filtration leading to a clear colourless solution. (C) DLS measurement and (D) UV/Vis absorbance spectra of micelles formulated with and without Nile Red. (E) Photograph of Nile Red loaded particles before and after degradation. (F) Lipase-mediated enzymatic degradation of Nile Red loaded mPEG$_{48}$-b-P(MDO)$_{71}$ micelles followed by the light scattering count rate. (G) Lipase-mediated Nile Red release from mPEG$_{48}$-b-P(MDO)$_{71}$ micelles followed by UV-vis absorbance at 549 nm.

massive increase in turbidity within the first 6 hours. Simultaneously, released Nile Red starts to adsorb to the bottom of the DLS cuvette. After one day, all drug-loaded micelles were fully degraded and solutions became colourless with the precipitated dye at the bottom (Fig. 6E and Fig. S56†).

As the UV absorbance of Nile Red is influenced by its solvation,[28–31] UV/Vis spectroscopy can also be used as a tool to monitor its release from the drug carrier over time. However, as the decrease in pH significantly influenced particle aggregation, UV/Vis spectroscopy could not be applied to those formulations to monitor dye release at acidic pH. Alternatively, enzymatic degradation in the presence of lipase at pH 7 did not afford particle aggregation (compare Fig. S57†) and was, therefore, applied to study dye release kinetics by both UV/Vis spectroscopy and DLS. Similarly to the findings shown in Fig. 5D, a rapid decrease in the light scattering count rate was found for the samples in the presence of lipase, confirming again similar degradation behaviour for both empty and dye loaded micelles (Fig. 6F). In parallel, UV/Vis spectroscopy confirmed what was observed visually with the naked eye (Fig. S57†). A rapid decrease in the Nile Red absorbance maximum around 549 nm (compare Fig. 6D) is found for the dye loaded micelles in the presence of lipase (Fig. 6G) corresponding to the enzyme-mediated release of Nile Red from the micelles. Without lipase only a sustained degradation of mPEG$_{48}$-b-P(MDO)$_{50}$ derived block copolymer

micelles (Fig. 6F) corresponding to a gradual release of encapsulated Nile Red over time (Fig. 6G) was detected at neutral pH.

3.8 Application as an immune drug delivery system

Prior to further investigations as suitable drug carriers, the *in vitro* cytotoxicity of the mPEG$_{48}$-b-P(MDO)$_{50}$ micelles was studied by MTT-assay on Raw Blue macrophages. Fig. 7D indicates that concentrations up of 400 μg mL^{-1} did not influence the viability (compared to PBS buffer as a negative control and 10% DMSO as a positive control). Encouraged by these results, an immunostimulating TLR agonist could be formulated into mPEG$_{48}$-b-P(MDO)$_{50}$ in analogy to Nile Red.

For this purpose, the amphiphilic TLR 7 agonist Adifectin was selected. Its molecular structure is composed of a hydrophilic TLR 7 interacting head group, a basic spermine linker (which might favour additional interaction with the negatively charged carboxylate end groups of the mPEG$_{48}$-b-P(MDO)$_{50}$ block copolymers) and two hydrophobic phytanyl groups that guarantee interaction with the hydrophobic cores of the mPEG$_{48}$-b-P(MDO)$_{50}$ derived micelles (compare Fig. S58†). It was fabricated into a polymer film with mPEG$_{48}$-b-P(MDO)$_{50}$ and then rehydrated with 120 mM phosphate buffer. Adifectin itself can also be formulated into water according to the manufacturer's guidelines assisted by ethanol. In both cases with and without mPEG$_{48}$-b-P(MDO)$_{50}$, all samples were sonicated
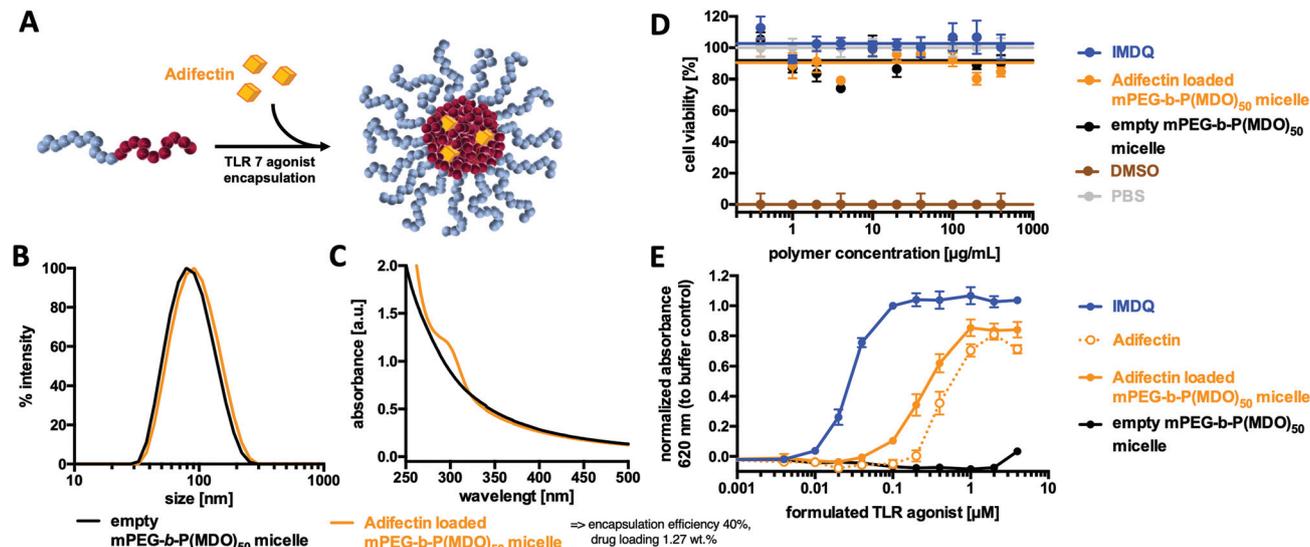
Fig. 7 Application of P(MDO) derived micelles as an immunodrug delivery system: (A) Schematic representation of drug loading of a TLR 7 agonist into micelles for drug delivery purposes. (B) Normalized micellar size distribution plot and (C) UV/vis absorbance spectra of micelles with and without Adifectin. (D) Cellular toxicity analysis of mPEG$_{48}$-b-PMDO$_{50}$ on Raw Macrophages determined by MTT assay (n = 4). (E) TLR stimulation assay on RAW Blue macrophages of Adifectin formulated with and without mPEG$_{48}$-b-PMDO$_{50}$. The imiquimod-analogue IDMQ serves as a positive control and empty micelles provide blank probes with no immunostimulation (n = 4).

and filtered through GHP-filters of 0.45 μm pore size prior to use.

Subsequent DLS measurement showed only a slight increase in micellar size for the loaded micelles, which can be seen as a first indication of successful immunodrug loading (Fig. 7B – note that Adifectin is an amphiphile and might probably be more incorporated into the particle interface than into the core, thus only slightly contributing to an increase in size). In addition, the UV/Vis spectrum in Fig. 7C further proves the successful formulation of Adifectin into the micelles. The drug load could be quantified by applying an external calibration curve (Fig. S61†), where micelles prepared without Adifectin served as a blank sample.

Subsequently, the ability of *in vitro* immune cell TLR 7 activation was determined by incubating RAW-Blue macrophages as the TLR 7 reporter cell line with different poly(esteracetal)/Adifectin concentrations (Table S2†). Interestingly, the formulation containing the amphiphilic polymer was more potent compared to the free drug, although the polymer solely did not show any immune stimulation (Fig. 7E). Additional quantification of the sample without a block copolymer by UV/Vis spectroscopy, as shown in Fig. S61,† revealed that the increased TLR stimulation activity results from an enhanced ability to solubilise Adifectin during preparation. In fact, the presence of the amphiphilic mPEG$_{48}$-b-P(MDO)$_{50}$ block copolymer promotes the drug's solubility in water and, thus, its accessibility to the TLR.

Retrospective correction of the determined Adifectin concentration according to Fig. S61† showed that formulations with mPEG$_{48}$-b-P(MDO)$_{50}$ micelles did not lose Adifectin's receptor activity and remained almost as potent as the free drug alone (Fig. S60 and Table S3†).

Furthermore, there was no indication of decreased cell viability on macrophages after treatment with the polymer formulation, as determined by MTT assay (Fig. 7D). Taken together, these findings suggest that amphiphilic TLR agonists were safely and efficiently formulated by the mPEG-b-P(MDO)$_{50}$ block copolymers and retained their drug activity on the TLR receptor in a micellar form. Consequently, the dual pH-degradable mPEG$_{48}$-b-P(MDO)$_{50}$ block copolymer system can be considered as a highly promising approach for such immunodrug molecules towards possible lymph node focused delivery strategies.

4. Conclusion

To the best of our knowledge, for the first time a variety of amphiphilic poly(esteracetal) diblock copolymers could successfully be synthesized and studied for their potential as immunodrug carrier systems.

For this purpose, reaction conditions for the cationic ring-opening polymerisation of cyclic esteracetal monomer 2-methyl-1,3-dioxan-4-one were optimised and then applied for block copolymer synthesis with methoxy poly(ethylene glycol) (mPEG) as the macroinitiator. Successful amphiphilic mPEG-b-P(MDO) block copolymer formation could be verified by several NMR and mass spectroscopy techniques as well as SEC analysis. By varying the monomer to initiator ratio, it was possible to obtain block copolymers with different hydrophobic block lengths between 15 and 71 monomer units.

All synthesized block copolymers could be self-assembled into well-defined monomodal micelles by direct hydration. Their sizes were highly reproducible under these conditions

and varied between 26 nm and 141 nm, covering the relevant size range for immunodrug delivery purposes (*e.g.* passive lymph node accumulation). A dual pH-responsive behaviour towards rapid particle degradation was confirmed by DLS and ^{1}H-NMR. While micelles remained stable at pH 7.2, HCl or NaOH addition as well as exposure to lipase led to immediate degradation.

In subsequent drug loading studies, Nile Read as a hydrophobic guest molecule could be loaded and released from the degradable amphiphilic block copolymers efficiently. Finally, first *in vitro* studies were conducted where no cellular toxicities were found on macrophages. An amphiphilic TLR-7 agonist (Adifectin) was co-formulated into the mPEG-*b*-P(MDO) block copolymer micelles and its activity was investigated by TLR stimulation of RAW Blue macrophages. The degradable amphiphilic block copolymer was able to solubilize Adifectin more efficiently and retained the drug's activity on the TLR receptor.

These findings suggest that mPEG-*b*-P(MDO) can be utilized for providing optimized delivery opportunities for promising immunodrug molecules, also towards possible lymph node focused delivery. In our ongoing research endeavours, we will focus on enhancing drug loading and micellar stability at neutral pH to prevent premature drug release before reaching its target site.

Conflicts of interest

There are no conflicts to declare.

Acknowledgements

References

1 (*a*) A. P. Singh, A. Biswas, A. Shukla and P. Maiti, *Signal Transduction Targeted Ther.*, 2019, **4**, 33; (*b*) S. Senapati, A. K. Mahanta, S. Kumar and P. Maiti, *Signal Transduction Targeted Ther.*, 2018, **3**, 7; (*c*) Y. Zhang, Y. Huang and S. Li, *AAPS PharmSciTech*, 2014, **15**, 862–871; (*d*) A. Z. Wang, R. Langer and O. C. Farokhzad, *Annu. Rev. Med.*, 2012, **63**, 185–198; (*e*) R. S. Riley, C. H. June, R. Langer and M. J. Mitchell, *Nat. Rev. Drug Discovery*, 2019, **18**, 175–196; (*f*) E. H. Chang, J. B. Harford, M. A. W. Eaton, P. M. Boisseau, A. Dube, R. Hayeshi, H. Swai and D. S. Lee, *Biochem. Biophys. Res. Commun.*, 2015, **468**, 511–517; (*g*) S. Mitragotri, P. A. Burke and R. Langer, *Nat. Rev. Drug Discov.*, 2014, **13**, 655–672.

2 M. Talelli, M. Barz, C. J. Rijcken, F. Kiessling, W. E. Hennink and T. Lammers, *Nano Today*, 2015, **10**, 93–117.

3 (*a*) H. Chen, C. Khemtong, X. Yang, X. Chang and J. Gao, *Drug Discovery Today*, 2011, **16**, 354–360; (*b*) Á. Tarcsay and G. M. Keserű, *J. Med. Chem.*, 2013, **56**, 1789–1795.

4 W. J. Gradishar, S. Tjulandin, N. Davidson, H. Shaw, N. Desai, P. Bhar, M. Hawkins and J. O'Shaughnessy, *J. Clin. Oncol.*, 2005, **23**, 7794–7803.

5 (*a*) K. S. Lee, H. C. Chung, S. A. Im, Y. H. Park, C. S. Kim, S.-B. Kim, S. Y. Rha, M. Y. Lee and J. Ro, *Breast Cancer Res. Treat.*, 2008, **108**, 241–250; (*b*) T. Chida, Y. Miura, H. Cabral, T. Nomoto, K. Kataoka and N. Nishiyama, *J. Controlled Release*, 2018, **292**, 130–140; (*c*) K. Kataoka, A. Harada and Y. Nagasaki, *Adv. Drug Delivery Rev.*, 2012, **64**, 37–48; (*d*) N. Nishiyama, Y. Matsumura and K. Kataoka, *Cancer Sci.*, 2016, **107**, 867–874.

6 G. M. Lynn, R. Laga and C. M. Jewell, *Cancer Lett.*, 2019, **459**, 192–203.

7 H. Cabral and K. Kataoka, *J. Controlled Release*, 2014, **190**, 465–476.

8 (*a*) H. Jiang, Q. Wang and X. Sun, *J. Controlled Release*, 2017, **267**, 47–56; (*b*) H. Cabral, Y. Matsumoto, K. Mizuno, Q. Chen, M. Murakami, M. Kimura, Y. Terada, M. R. Kano, K. Miyazono, M. Uesaka, N. Nishiyama and K. Kataoka, *Nat. Nanotechnol.*, 2011, **6**, 815–823; (*c*) N. J. Butcher, G. M. Mortimer and R. F. Minchin, *Nat. Nanotechnol.*, 2016, **11**, 310–311; (*d*) Z. Zhao, A. Ukidve, V. Krishnan and S. Mitragotri, *Adv. Drug Delivery Rev.*, 2019, **143**, 3–21; (*e*) K. Miyata, R. J. Christie and K. Kataoka, *React. Funct. Polym.*, 2011, **71**, 227–234.

9 M. L. Etheridge, S. A. Campbell, A. G. Erdman, C. L. Haynes, S. M. Wolf and J. McCullough, *Nanomedicine*, 2013, **9**, 1–14.

10 (*a*) J. Azzi, Q. Yin, M. Uehara, S. Ohori, L. Tang, K. Cai, T. Ichimura, M. McGrath, O. Maarouf, E. Kefaloyianni, S. Loughhead, J. Petr, Q. Sun, M. Kwon, S. Tullius, U. H. von Andrian, J. Cheng and R. Abdi, *Cell Rep.*, 2016, **15**, 1202–1213; (*b*) E. Hong and M. A. Dobrovolskaia, *Adv. Drug Delivery Rev.*, 2019, **141**, 3–22.

11 (*a*) B. J. Ignacio, T. J. Albin, A. P. Esser-Kahn and M. Verdoes, *Bioconjugate Chem.*, 2018, **29**, 587–603; (*b*) G. M. Lynn, R. Laga, P. A. Darrah, A. S. Ishizuka, A. J. Balaci, A. E. Dulcey, M. Pechar, R. Pola, M. Y. Gerner, A. Yamamoto, C. R. Buechler, K. M. Quinn, M. G. Smelkinson, O. Vanek, R. Cawood, T. Hills, O. Vasalatiy, K. Kastenmüller, J. R. Francica, L. Stutts, J. K. Tom, K. A. Ryu, A. P. Esser-Kahn, T. Etrych, K. D. Fisher, L. W. Seymour and R. A. Seder, *Nat. Biotechnol.*, 2015, **33**, 1201–1210; (*c*) P. J. Pockros, D. Guyader, H. Patton, M. J. Tong, T. Wright, J. G. McHutchison and T.-C. Meng, *J. Hepatol.*, 2007, **47**, 174–182; (*d*) P. Savage, V. Horton, J. Moore, M. Owens, P. Witt and M. E. Gore, *Br. J. Cancer*, 1996, **74**, 1482–1486.

12 L. Nuhn, N. Vanparijs, A. de Beuckelaer, L. Lybaert, G. Verstraete, K. Deswarte, S. Lienenklaus, N. M. Shukla,

A. C. D. Salyer, B. N. Lambrecht, J. Grooten, S. A. David, S. de Koker and B. G. de Geest, *Proc. Natl. Acad. Sci. U. S. A.*, 2016, **113**, 8098–8103.

13 S. Van Herck, K. Deswarte, L. Nuhn, Z. Zhong, J. P. Portela Catani, Y. Li, N. N. Sanders, S. Lienenklaus, S. De Koker, B. N. Lambrecht, S. A. David and B. G. De Geest, *J. Am. Chem. Soc.*, 2018, **140**, 14300–14307.

14 S. Keller, J. T. Wilson, G. I. Patilea, H. B. Kern, A. J. Convertine and P. S. Stayton, *J. Controlled Release*, 2014, **191**, 24–33.

15 H. Wu, V. Estrella, P. Enriquez-Navas, A. El-Kenawi, S. Russell, D. Abrahams, A. Ibrahim-Hashim, D. Longo, Y. Reshetnyak, K. Luddy, M. Damaghi, S. R. Pillai, M. Beatty, S. Pilon-Thomas, P. Swietach and R. J. Gillies, Lymph Nodes Inhibit T-cell Effector Functions Locally by Establishing Acidic Niches, *bioRxivorg*, 2019, DOI: 10.1101/689604.

16 (*a*) R. T. Martin, L. P. Camargo and S. A. Miller, *Green Chem.*, 2014, **16**, 1768–1773; (*b*) S. A. Miller and R. T. Martin, *U.S. Pat.*, WO2010/065641, 2010; (*c*) A. E. Neitzel, L. Barreda, J. T. Trotta, G. W. Fahnhorst, T. J. Haversang, T. R. Hoye, B. P. Fors and M. A. Hillmyer, *Polym. Chem.*, 2019, **10**, 4573–4583; (*d*) A. Hufendiek, S. Lingier and F. E. Du Prez, *Polym. Chem.*, 2019, **10**, 9–33.

17 A. E. Neitzel, M. A. Petersen, E. Kokkoli and M. A. Hillmyer, *ACS Macro Lett.*, 2014, **3**, 1156–1160.

18 A. E. Neitzel, T. J. Haversang and M. A. Hillmyer, *Ind. Eng. Chem. Res.*, 2016, **55**, 11747–11755.

19 A. K. Covington, M. Paabo, R. A. Robinson and R. G. Bates, *Anal. Chem.*, 1968, **40**, 700–706.

20 P. Olsén, K. Odelius and A.-C. Albertsson, *Biomacromolecules*, 2016, **17**, 699–709.

21 P. Kubisa and S. Penczek, *Prog. Polym. Sci.*, 1999, **24**, 1409–1437.

22 (*a*) S.-D. Li and L. Huang, *J. Controlled Release*, 2010, **145**, 178–181; (*b*) K. Knop, R. Hoogenboom, D. Fischer and U. S. Schubert, *Angew. Chem., Int. Ed.*, 2010, **49**, 6288–6308.

23 A. Schudel, D. M. Francis and S. N. Thomas, *Nat. Rev. Mater.*, 2019, **4**, 415–428.

24 C. Oussoren, J. Zuidema, D. J. A. Crommelin and G. Storm, *Biochim. Biophys. Acta, Biomembr.*, 1997, **1328**, 261–272.

25 Y. Mai and A. Eisenberg, *Chem. Soc. Rev.*, 2012, **41**, 5969–5985.

26 Y. Zhu, B. Yang, S. Chen and J. Du, *Prog. Polym. Sci.*, 2017, **64**, 1–22.

27 H. S. Choi, W. Liu, P. Misra, E. Tanaka, J. P. Zimmer, B. Itty Ipe, M. G. Bawendi and J. V. Frangioni, *Nat. Biotechnol.*, 2007, **25**, 1165–1170.

28 J. Jiang, X. Tong and Y. Zhao, *J. Am. Chem. Soc.*, 2005, **127**, 8290–8291.

29 S. Binauld and M. H. Stenzel, *Chem. Commun.*, 2013, **49**, 2082–2102.

30 P. Greenspan and S. D. Fowler, *J. Lipid Res.*, 1985, **26**, 781–789.

31 J. Bigot, B. Charleux, G. Cooke, F. Delattre, D. Fournier, J. Lyskawa, L. Sambe, F. Stoffelbach and P. Woisel, *J. Am. Chem. Soc.*, 2010, **132**, 10796–10801.